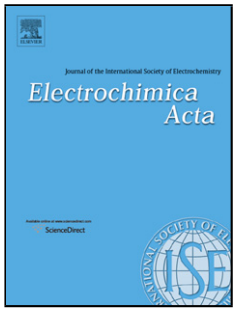

Title: Durable Membrane Electrode Assemblies for Proton Exchange Membrane Electrolyzer Systems Operating at High Current Densities

Author: P. Lettenmeier R. Wang R. Abouatallah S. Helmly T. Morawietz R. Hiesgen S. Kolb F. Burggraf J. Kallo A.S. Gago K.A. Friedrich

PII: S0013-4686(16)31016-7
DOI: http://dx.doi.org/doi:10.1016/j.electacta.2016.04.164
Reference: EA 27199

To appear in: *Electrochimica Acta*

Received date: 13-1-2016
Revised date: 27-4-2016
Accepted date: 27-4-2016

Please cite this article as: P.Lettenmeier, R.Wang, R.Abouatallah, S.Helmly, T.Morawietz, R.Hiesgen, S.Kolb, F.Burggraf, J.Kallo, A.S.Gago, K.A.Friedrich, Durable Membrane Electrode Assemblies for Proton Exchange Membrane Electrolyzer Systems Operating at High Current Densities, Electrochimica Acta http://dx.doi.org/10.1016/j.electacta.2016.04.164

Durable Membrane Electrode Assemblies for Proton Exchange Membrane Electrolyzer Systems Operating at High Current Densities

P. Lettenmeier[1], R. Wang[2], R. Abouatallah[2], S. Helmly[1], T. Morawietz[3], R. Hiesgen[3], S. Kolb[1], F. Burggraf[1], J. Kallo[1,4], A. S. Gago[1*] aldo.gago@dlr.de, K. A. Friedrich[1,5]

[1]Institute of Engineering Thermodynamics, German Aerospace Center, Pfaffenwaldring 38-40, Stuttgart, 70569, Germany

[2]Hydrogenics Corporation, 220 Admiral Boulevard, Mississauga, ON L5T 2N6, Canada

[3]University of Applied Sciences Esslingen, Dep. of Basic Science, Kanalstrasse 33, Esslingen, 73728, Germany

[4]Institute of Energy Conversion and Storage, University of Ulm, Helmholtzstr. 18, Ulm, 89081, Germany

[5]Institute of Energy Storage, University of Stuttgart, Keplerstraße 7, Stuttgart 70174, Germany

[*]Corresponding author: Tel.: +49 711 6862-8090, fax: +49 711 6862-747.

Graphical Abstract

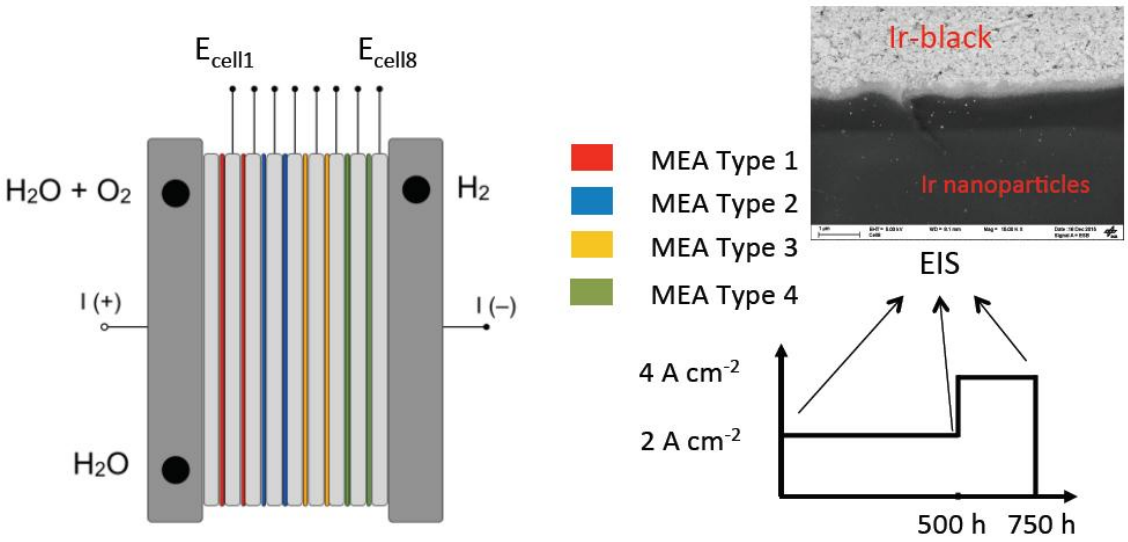

Abstract

High efficiencies, wide operation range and rapid response time have motivated the recent interest in proton exchange membrane (PEM) electrolysis for hydrogen generation with surplus electricity. However, degradation at high current densities and the associated mechanism has not been thoroughly explored so far. In this work, membrane electrode assemblies (MEA) from different suppliers are aged in a commercial PEM electrolyzer (2.5 N m^3 H_2 h^{-1}), operating up to 4 A cm^{-2} for more than 750 h. In all cases, the cell voltage (E_{cell}) decreases during the testing period. Interestingly, the cells with Ir-black anodes exhibit the highest performance with the lowest precious metal loading (1 mg cm^{-2}). Electrochemical impedance spectroscopy (EIS) shows a progressive decrease in the specific exchange current, while the ohmic resistance decreases when doubling the nominal current density. This effect translates into an enhancement of cell efficiency at high current densities. However, Ir concurrently leaches out and diffuses into the membrane. No decrease in membrane thickness is observed at the end of the tests. High current densities do not lead to lowering the performance of the PEM electrolyzer over time, although MEA components degrade, in particular the anode.

Keywords: PEM electrolyzer; PEM electrolysis system; MEA; Degradation; Impedance spectroscopy; High current density; Accelerated stress tests

1. Introduction

Since December 2015, 195 countries adopted the first universal climate agreement at the United Nations conference on climate change (COP21). It establishes to hold the increase in the global average temperature below 2 °C by reducing emissions to 40 gigatonnes of CO_2 [1]. A major emitting sector is the energy sector and renewable sources such as wind, water, and solar can help reduce the emissions. In this context, Germany with its energy policy of *Erneuerbare Energien Gesetz* – EEG targets to produce 80% of electrical power from renewables by 2050 [2]. However, due to the substantial discrepancy between the temporal availability of renewable energy (e.g. differences between day/night or winter/summer) and the actual needs, the opportunity of temporarily store excess energy is necessary. In such scenario, hydrogen can act as a carbon neutral energy vector when being produced by water electrolysis using surplus electricity from renewables [3]. Commercially, hydrogen can electrochemically be produced by alkaline and proton exchange membrane (PEM) electrolysis [4], representing both environmentally friendly but economically unattractive technologies if natural gas infrastructure for steam reforming is available. Despite the fact that alkaline electrolysis is a well-established and durable technology, the issues in gas purity, safety and response time has pushed the research and the industrial interest toward the PEM technology in the recent years [5,6]. For comparision alkaline electrolyzers can produce H_2 up to 99.5% purity while 99.995 % can be achieved with the PEM technology [7]. Moreover, PEM electrolyzers have a relevant technological potential because of the high efficiency, compact design, simplicity of the system ancillary, easy maintenance, rapid response and wide dynamic operation range [6,8–12]. However, questions about durability, degradation mechanism and availability of precious metals

for catalyst are still unanswered. Furthermore, the high investment cost hinders the wide spread commercialization of the technology at the Mega- or Terawatt scale.

Currently, the investment costs of a PEM electrolyzer system are almost three times higher compared to the alkaline technology [13]. The stack comprises about 60% of the cost of the PEM electrolyzer system and the titanium bipolar plates (BPP), are responsible for half the cost of the stack. While membrane electrode assembly (MEA) manufacture and the precious metal catalysts own together about 20% [14]. Yet, the investment cost of the PEM electrolysis technology is to be decreased from 1000 – 2000 €/kW to 300-600 €/kW in 2030 [11,15]. One approach to meet this target is by reducing the stack component cost. For example, BPPs are manufactured on titanium thanks to its corrosion stability in oxidative environments, but machining this metal is complicate and expensive [16,17]. Recently, coated stainless steel has proven to be an alternative base material for BPPs, showing similar durability than the titanium ones [18,19].

Once the problem of the high cost of the bipolar plates is overcome then the precious metal catalysts will be the dominant constraint. Platinum is commonly used as hydrogen evolution reaction (HER) catalyst at the cathode and iridium is used as oxygen evolution reaction (OER) catalyst at the anode [20,21]. The former requires much higher loadings than platinum and is expensive ($545.95 per troy ounce, national minerals information center, 2015). Moreover, it is one of the scarcest elements with an annual production value of less than 9 tons [22]. It certainly will not be sufficient for a Terawatt infrastructure of PEM electrolyzers with the current loadings of 2-3 mg cm^{-2} [23]. In this context, several groups are intensively working on the development of highly active OER catalyst with less amount of Ir [24–31] or eve Ir-free catalysts [32].

Finally, another approach for reducing the investment cost of the stack is simply by operating it at high current densities. Nowadays most commercially available PEM electrolyzers are designed for operating at current densities lower than 2 A cm^{-2} (nominal). Assuming an ideal faradic efficiency (ε_F) of 100%, an increase of the current density from 2 to 4 A cm^{-2} would double the hydrogen production but not affect the cost of the stack. Only the adjustment of the power electronics and ancillary parts is required, which contribute moderately to the system cost. Yet, the behavior of a PEM electrolyzer system and degradation of MEAs operating at high current densities is still unclear. In this work rainbow stacks with MEAs from different suppliers were tested in a commercial PEM electrolyzer (2.5 N m^3 H_2 h^{-1}) up to 4 A cm^{-2} for more than 750 h under constant and dynamic regimes. The stack performance and degradation mechanisms are thoroughly addressed.

2. Experimental

2.1. PEM electrolyzer system

The commercially available Hylyzer® Hydrogen Generator (HHG) from Hydrogenics was used as a test bench. This system designed for 40-cell stack with an active area of 120 cm^2 for operation at a nominal current density of 2 A cm^{-2} with an overall production of 2.5 Nm^3 h^{-1}. System modifications from Hydrogenics allowed reaching a peak current density up to 6 A cm^{-2} with an 8-cell stack, although the overall system efficiency is compromised. The 92E stack model technology from Hydrogenics was used for the measurements. Several MEAs from different suppliers were assembled to investigate the impact of catalysts, electrode layer and production process. All the MEAs had the same membrane Nafion 115 and therefore same

thickness. As customized MEA (E500) with Ir-black (Umicore) as oxygen evolution reaction (OER) catalyst was manufactured since this material is one of most active commercially available catalyst [33]. A detailed summary of the MEA specifications is given in Table 1.

2.2. Protocol of measurements

An initial activation time for more than 300 h at nominal conditions was employed for reaching a stable condition. Subsequently, a protocol of measurements was implemented for studying performance and degradation of the stack. Figure 1a and 1b show the stack current density and the potential response, respectively, with respect to operating time. Initially, electrochemical impedance spectroscopy (EIS) for each cell was performed at 0.25 A cm^{-2} before set point T1. Thereafter the HHG operated constantly at 2 A cm^{-2} for more than 400 h and then 50 h dynamically with a maximum (j_{max}) and minimum (j_{min}) current densities of 2 A cm^{-2} and 0.15 A cm^{-2}, accordingly. EIS was performed again before (T2) and after (T3) operation at constant 4 A cm^{-2} for 250 h. In case of cell 7 and 8, EIS measurements were performed at different current densities to gain more information about the kinetic behavior. These were performed on each cell of the stack with an external EIS module. For this purpose, the stack was disconnected from the rectifier and only the water pump of the anodic cycle was running.

2.3. Post-mortem analysis of MEA with Ir-black

2.3.1. Atomic force microscopy (AFM)

For the AFM investigations, a Bruker Multimode 8 AFM (Karlsruhe, Germany), equipped with a Nanoscope V controller, a closed loop scanner with open loop Z-axis (nPoint, USA) and current amplifier (PeakForce-TUNA™, Bruker Corp., USA) was used. Cross sections of the MEA

samples were embedded in polyurethane, cut by microtome and analyzed in a closed chamber, where the relative humidity (RH) was set to (25 ± 5) %. For current recording, the samples were fixed with conductive tape to the steal sample holder. A voltage of 40 mV was applied between sample holder and AFM probe, with the AFM probe at ground. Using PtIr-coated tips (PPP-NCHPt, 42 N/m; Nanosensors), the current measured in tapping mode was averaged by a lock-in amplifier (PF-TUNA Module, Bruker, USA). This mode enables simultaneous retrieval of nano-mechanical information and current. All images were scanned at areas of 5 µm² with 1024 points/ line resulting in a pixel size of 4.88 nm. The relative conductive area was evaluated by the Nanoscope Analysis software V 1.6 using bearing analysis.

2.3.2. Scanning electron microscopy (SEM)

To determine the thickness of the membrane and changes in the electrodes, pristine and *post mortem* MEA cross-sections were examined with SEM. Samples with a width (i.e., cross-sectional length) of approximately 3 mm were cut from a pristine MEA and from two MEAs after tests in the HHG. The MEA cross-sections were prepared via freeze-fractioning in liquid nitrogen. SEM measurements were conducted with an ULTRA plus (Zeiss Corp.) scanning electron microscope. The images were recorded based on secondary electrons (SE) and backscattered electrons (BE) at a voltage of 5 kV. The resolution of the SEM was 1.0 nm at 15 kV and 1.7 nm at 1 kV. Each cross-section was investigated at three different positions. At each position, the thicknesses of the membrane and electrode layers were measured at three random spots. Therefore, each presented thickness value is the average of nine single values.

3. Results and discussion

3.1. Performance of the electrolyzer

The cell voltage (E_{cell}) - current characteristics of the cell 1-8 with different providers is presented in Figure 2a. The right axis corresponds to the temperature of stack *vs.* the applied current density. The stack temperature in the HHG is controlled by its own generated heat and cools down with air ventilation, which turns on when reaching the temperature limit of 63°C. Thereafter, it operates with the fans turned on until the temperature drops down to 55°C, thus causing temperature induced fluctuations in the E_{cell}. The higher the current density of the stack, the higher are the over potentials and the corresponding temperature-dependent power losses (Figure S1, supporting information). When performing the polarization curve, the temperature variations lead to a bending of the current-potential curve, in particular at high current densities, until the ventilation starts at around 3.85 A cm^{-2}. Then the stack cools down and the potential increases again.

Figure 2b shows the initial EIS for each cell at 30 A, which corresponds to a current density of 0.25 A cm^{-2}. It can be clearly observed, that cell 7 and cell 8, the two cells with Ir-black as an anode catalyst has the smallest ohmic resistance, which is represented by the x-axis intersection of the Nyquist diagram, Figure 2b, and the lowest activation resistance observed by the smallest value for the impedance of the second semi cycle, Figure 2c. The ohmic resistance varies about ± 0.04 Ω cm^2 even though the MEAs have same membrane thickness. The small variations in the ohmic resistance are within the experimental range and can be originated in difference in the catalyst layer thickness, discrepancies of contact with the current collector, or assembly issues during the manufacturing process. The catalyst has an influence as well in the ohmic resistance

but is smaller. The mayor contribution for reducing the E_{cell} is attributed to kinetic behavior of the anode catalyst, Figure 2b. The EIS results are in a good agreement with the recorded polarization curve in Figure 2a, in which cell 7 and 8 show the highest performance. Compared to the other cells, a significant reduction of catalyst material and simultaneously an improvement of performance are achieved with the Ir-black catalyst. The rest of the MEAs contain thermally oxidized IrO_2 but the exact nature of the catalyst was not disclosed by the supliers. Rotating disc electrode (RDE) measurements in Figure S2 were performed to confirm the high OER activity of the Ir-black catalyst of Cell 7 and 8.

Figure 3a shows the cell potential (E_{cell}) of cell 7 and 8 at 2 A cm^{-2} during 400 h of operation. One can observe a large variation of the measured E_{cell}, Figure 3a, due to temperature fluctuations. The temperature induced oscillations of ± 1.5 °C in Fig. 3a are caused by the addition of fresh water into the stack, which also serves as coolant. When the electrolyzer is operated at 4 A cm^{-2}, Fig. 3b, the periodic turn on-off of the fan, which cools then entire system enclosure, produces variations in temperature up to ± 4 °C. An average E_{cell} of 1.94 V was measured at 2 A cm^{-2} and 2.27 V at 4 A cm^{-2}.

In general the performance of all cells is quite remarkable, being above of what it has been previously reported for PEM electrolyzer systems with comparable cell sizes, temperature, membrane thickness and H_2 production rate [6,8,34–39]. To get some insight about the stability of the MEAs, polarization curves and impedance spectra were recorded before (T1) and after (T2) running the HHG at 2 A cm^{-2} for ca. 500 h, Figure 3a, and after 250 h at 4 A cm^{-2} (T3), Figure 3b. A first trend of improving efficiency over time can be observed in both, Figure 3b, at 2 and 4 A cm^{-2}, respectively. More precisely, it can be shown in Figure 3c where the initial

performance at T1 is taken out of the first polarization curve and compared with the performance at 2 A cm^{-2} at T2 and T3. The other MEAs are included as well for comparison purposes. Here again the lowest E_{cell} was obtained with the Ir-black anode. The result is interesting because the rest of the MEAs have thermally treated IrO_2. Recently, fundamental studies have shown that the Ir oxy-hydroxides, which forms on metallic Ir, are very active for OER [33,40–42]. Our results are in good agreement with these reports. Figure 3c depicts as well that for all MEAs the efficiency improves as E_{cell} decreases over time. These effects contradicts other reports, where degradation rates of 1.5 up to 35.5 μV h^{-1} were measured [43,44] and suggest that the MEAs do not experience any degradation. In the next sections EIS is used to separate several degradation effects, combined with X-ray photoelectron spectroscopy (XPS) analysis of the DI water resin and SEM and AFM cross-section imaging for *post mortem* analysis. The results obtained with customized MEAs with Ir-black anodes (cell 7 and 8) will serve for further discussions since they showed the lowest E_{cell} at any current density. The other MEAs contain thermally oxidized IrO_2 but the exact nature of the catalyst is not disclosed.

3.2. Electrochemical impedance spectroscopy

Figure 4a presents the equivalent circuit used for simulating the impedance spectra for quantitative comparison. The element R1 is an ohmic resistor, which accounts for the ohmic parts of the PEM electrolyzer cells such as electrical or ionic conductive elements. It corresponds mostly to the high frequency (HF) x-axis interception at ca. 1 kHz. Two R/CPE semi circuits model the two arcs shown in Figure 4b. The meaning of the first arc at high frequencies is controversially discussed in the literature. Taking into account, that PEM electrolysis and PEM

fuel cell operations are often interpreted analogously, the high frequency arc could explained by the second electrochemical process corresponding to the hydrogen evolution reaction (HER) [45,46]. Other groups associate the HF arc with charge transfer processes combined with double layer effects of electrical and/or ionic conductive materials and oxides in the active layer [47–49]. We support the interpretation of the latter in order to explain the small impact of the current density on the HF arc and the linear resistance behavior. This resistance increases after reaching higher potentials (at T3), which can be attributed to morphology and structure changes in the electrode (Figure S3, supporting information). Figure 4b shows the impedance spectra of cell 7 at T1, T2 and T3 including the simulation fitting. The most obvious trend is the decrease of ohmic resistance over time. Figure 4c shows the EIS measurements at different current densities, which are also carried out for cell 7 and cell 8. The results provide detailed information about kinetic parameters, such as the Tafel slope and specific exchange current.

Detailed analysis of the impedance spectra was exemplary made for cell 7, Figure 5a-5d. The polarization curves presented in Figure 5a were corrected by a factor of 5.5 mV $°C^{-1}$ to eliminate the impact of the small temperature difference. The temperature correction was not necessary for the EIS measurements and the polarization curves in Figure 5b. These measurements were performed shutting off completely the H_2-generator and an external pump with low flow rates along with a potentiostat/galvanostat were used. Thus the temperature was strictly controlled at 29 ± 0.5 °C.

Figure 5a shows the polarization curves up to 2 A cm^{-2} at T1, T2 and T3 as summarized in

Table 2. Caused by a pronounced change in slope, the three curves intercept in the low current density regime, thus resulting in an increased potential at current densities lower than 0.5 A cm^{-2}. An improved performance can be observed at current densities higher than 0.75 A cm^{-2}. After 500 h of operation at constant 2 A cm^{-2} the stack shows a negative voltage decrease of -26 mV at 2 A cm^{-2} resulting in an average voltage decrease rate of -51.98 µV h^{-1}. A comparable rate of -40µV h^{-1} is obtained after 250 h of operation at 4 A cm^{-2} leading to an overall voltage change of -35.5 mV after 750 h. From these results, no degradation, i.e. voltage increase, was observed.

Figure 5b presents in detail the low current density regime below 0.33 A cm^{-2}. While an increase in performance is observed at higher current densities, we obtain a constant average degradation rate of ca. 13 µV h^{-1} at 0.25 A cm^{-2} during measurement time. The time dependence of the activation overpotential and the ohmic contributions to the voltage losses are depicted in Figure 5c and 5d, respectively. The degradation rates obtained from the analysis of the charge transfer resistance of the second arc in the EIS spectrum are the same for both operating strategies. Constant operation at 2 A cm^{-2} for 500 h causes a subsequent voltage increase of 6.2 mV measured at 0.25 A cm^{-2}, corresponding to a degradation rate of 12.4 µV h^{-1}. An operation of 250 h at 4 A cm^{-2} causes a 3.7 mV activation voltage degradation and a rate of 14.8 µV h^{-1}, again measured at 0.25 A cm^{-2}.

Deeper analysis of the kinetic properties and the changes over time can be made by ohmic drop correction. This procedure allows the analysis of the Tafel slopes and thus determination of the kinetic parameters, which are summarized in Table 2. It summarizes the Tafel slope and specific exchange current of the Buttler Volmer equation of cell 7 at T1, T2 and T3. The EIS measurements at 10, 20 30 and 40 A were used for analyzing the kinetic parameters. For the first measurement at T1, a Tafel slope of 44.3 mV dec^{-1} was calculated, being slightly higher

compared to the measurements of T2 and T3. The higher Tafel slope of T1 compared to T2 and T3, affects the specific exchange current. By correcting the linear fit of the logarithm scale to reach a comparable value for the slope of T1, the exchange current density shows a progressive degradation, which correlates very well with the data of Figure 5c. The increase of the charge transfer resistance, which lowers of the specific exchange current, is related to loss in electrocatalytic properties, e.g. decrease of surface area by losing catalyst material and ionomer in the catalyst layer. The presence of iridium in the DI water resin after the measurement protocol supports this conclusion. A list of all the elements detected by XPS analysis on the resin is given in Table 3, which were determined by XPS (Figure S4, supporting information).

In Figure 5d the decrease of the ohmic resistance over time (right axis, dotted lines) and the subsequent ohmic contributions to the overvoltage (left axis, straight lines) are shown in relation to the current density. In the first 500 h of operation at 2 A cm^{-2}, the ohmic resistance shows a decrease of 7 μΩ (recorded at 0.25 A cm^{-2}) compared to the initial value. This decrease is related to the applied current density as confirmed by an additional decrease of 30 μΩ after 250 h operation at 4 A cm^{-2}. The ohmic resistance of the stack is the sum of all ohmic behavior resistances such as ionic and electric resistances. In addition, its time dependence determining is the sum of ageing contributions. Degradation effects of interconnector material such as BPPs or current collectors should have a negative effect and should increase the ohmic resistance due to formation of semiconductive oxides or degradation of coatings. Therefore, the main impact of the ageing related to ohmic behavior is some change in the ionic conductive material. Positive impacts for the efficiency of PEM electrolysis determined by lower ohmic resistance could appear by continuous activation of the membrane by forming larger ionic conductive paths, which can also apply to the electrodes. Thinning of the membrane (not observed, see section 3.3)

or improving contacts between BPP, current collector and electrode can be reasons as well. An increase of S, F and O in DI water resin, Table 3, indicates a degradation of the ionic conductive omponent. However, the fluoride found in the resin could be due to MEA break-in (others call it "MEA conditioning") and the release of F may cease with time. Lastly, an increase of Fe and Ti content was also observed but it was minimal, considering the molar weight of the elements. The increase of Si can be explained by the degradation of the sealing material.

Summarizing, EIS measurements were proven to be a very useful tool for a deep analysis of the aging of MEAs and their performance. It was possible to separate the ohmic resistance from the activation overpotential and elucidate a degradation mechanism, which would not be obvious from the polarization and time dependent curves. By performing the EIS at different current densities we were able to get information on kinetic parameters such as specific exchange current and Tafel slopes, which helps to understand aging effects of the electrode layer. However, the strong influence of the decrease of ohmic resistance at high current density cannot be sustained without additionally *post mortem* analysis of the MEAs.

3.3. Degradation of MEAs

The *post mortem* MEAs with Ir-black anodes were analyzed by SEM and AFM in order to explain the changes of the ohmic resistance and propose a degradation mechanism before and after the testing protocol of Figure 1. Firstly, no decrease of membrane thickness was observed from cross-section SEM images. One reason the *post mortem* MEA is still having residual moisture and the swelling of the membrane could not be reduced. However, repetitive measurements with different specimens of the MEA proved that there is in fact no membrane

thinning contrary to what has been reported for PEM fuel cells and electrolyzers [50,51]. Whether we would expect membrane thinning in a test of less than 1000 h up to 4 A cm^{-2} is difficult to answer without further analysis. From PEM fuel cell studies, it was found that chemical membrane degradation depends strongly on the operation condition, especially on current density [52]. The observation that the fluorine release rate (FER) decreases with increasing current can be explained with the influence of gas crossover. High reactant concentrations increase membrane degradation [53,54]. Therefore, in PEM fuel cells, membrane degradation is relatively high at open circuit voltage (OCV), where the reactant concentration is high due to the fact that reactants are not being consumed. For PEM electrolysis, it should be opposite which means gas concentration is lowest at voltages close to 1.4 V and therefore it can be expected that the degradation is low. However at high current densities, gas concentration increases and one would expect degradation and membrane thinning. Membrane thinning in PEM electrolyzers occurs during long term operation even when using thick membranes as Nafion 117 [51], but so far it is not well understood the cause and in which operation conditions the effect is accelerated.

Figure 5b shows a release of catalyst particles into the membrane. Catalyst ions diffuse into the membrane and are reduced within the polymer which has also been reported for fuel cell MEAs [55–59]. Interesting is an interlayer between the catalyst layer and the membrane of about 5µm. Since this layer cannot be detected for the unused MEA, it is likely a diffusion of dissolved iridium into the membrane during operation.

The cross sections of the samples were also analyzed by material-sensitive and conductive AFM. The structure and the relative conductive area of the electrodes, determined by the NanoScope software on an area of 25 μm^2 were measured before and after operation. Before operation, the

conductive area of the anode and cathode was determined from three different areas to an average of 30 ± 4 % and 37 ± 2 %, respectively. After operation, the conductive area of the anode increased by approximately 50% while the conductive area of the cathode remained the same. The results of the AFM analysis are summarized in Table 4. Figure 7 shows the electrical conductivity AFM images on MEAs before and after operation. The images of the pristine MEAs are characterized by large non-conductive areas, which can be associated with the ionomer. Apart from the ionomer-rich areas, the conductive catalyst particles are homogenously distributed. After operation, agglomerates of catalyst particles can be observed in all areas investigated in the anodes of cell 7, Figure 7b, and cell 8, Figure 7c, and these are larger than in the pristine surface, Figure 7a. Conversely, the cathode side of both cells, Figure 7e and 7f, did not changed after operation compared with the initial state, Figure 7d. The AFM analysis confirms that the surface conductivity of the catalyst layer changed due to ionomer loss. It justifies the decrease of ohmic resistance, which only occurred when the electrolyzer operated at twice the nominal condition of current density.

4. Conclusions

A first insight on the degradation mechanism of PEM electrolyzers operating at high current densities has been provided. A commercial H_2-generator with a rainbow 8-cell stack having MEAs from different companies was operated up to 4 A cm^{-2} for this study. We showed that the aging of the PEM electrolyzer MEAs depends on current density and operation time, but the associated degradation mechanisms are different in each case. The operation at high current densities reduced the ohmic drops, while long operation led to gradual deactivation of the anode. *Post mortem* analysis of the MEAs (SEM and AFM) and water resin (XPS) revealed a current dependent loss of ionomer and catalyst material in the anode, which resulted in an unexpected

enhancement of cell performance at high current densities. Indeed, the current-potential curves of the cells showed a concomitant decrease in E_{cell} for all MEAs, which was caused by the aforementioned decrease in resistance. Remarkably, the MEA with the lowest Ir catalyst loading (1 mg cm^{-2}) showed the lowest E_{cell} at any current density. The development of durable MEAs for PEM electrolyzers is still a challenge and causes of degradation are yet to be comprehended. Lastly, besides the MEA degradation phenomena presented herein, thermal and mechanical stress during operation at high current densities, can cause additional reduction of the electrode surface area as it occurs in PEM fuel cells [53,60–62].

Acknowledgements

The authors acknowledge the Federal Ministry for Economic Affairs and Energy (BMWi) for financial support in the project No. 0325440A. We also thank Anke Steinhilber, and Pawel Gazdzicki for XPS analysis and Jörg Bürkle for his technical support in the electrochemical measurements.

References

[1] United Nations, Adoption of the Paris Agreement, (2015).

[2] Federal Ministry of Economic affairs (BMWi) - Germany, Gesetz für den Ausbau erneuerbarer Energien - EEG, (2014).

[3] A. Sternberg, A. Bardow, L. Bertuccioli, A. Chan, D. Hart, F. Lehner, et al., Power-to-What? – Environmental assessment of energy storage systems, Energy Environ. Sci. 8 (2015) 389–400. doi:10.1039/C4EE03051F.

[4] P. Millet, S. Grigoriev, Hydrogen from water electrolysis, in: L.M.G.A.M. Diéguez (Ed.), Renew. Hydrog. Technol., Elsevier Ltd, Amsterdam, 2013.

[5] J. Eichman, K. Harrison, M. Peters, Novel Electrolyzer Applications: Providing More Than Just Hydrogen, 2014.

[6] M. Carmo, D.L. Fritz, J. Mergel, D. Stolten, A comprehensive review on PEM water electrolysis, Int. J. Hydrogen Energy. 38 (2013) 4901–4934. doi:10.1016/j.ijhydene.2013.01.151.

[7] K. Zeng, D. Zhang, Recent progress in alkaline water electrolysis for hydrogen production and applications, Prog. Energy Combust. Sci. 36 (2010) 307–326. doi:10.1016/j.pecs.2009.11.002.

[8] K.E. Ayers, C. Capuano, E.B. Anderson, Recent Advances in Cell Cost and Efficiency for PEM-Based Water Electrolysis, ECS Trans. 41 (2012) 15–22. doi:10.1149/1.3684798.

[9] K.E. Ayers, L. Moulthrop, E.B. Anderson, E.C.S. Transactions, T.E. Society, Hydrogen Infrastructure Challenges and Solutions, ECS Trans. 41 (2012) 75–83. doi:10.1149/1.4729183.

[10] F. Barbir, PEM electrolysis for production of hydrogen from renewable energy sources, Sol. Energy. 78 (2005) 661–669. doi:10.1016/j.solener.2004.09.003.

[11] L. Bertuccioli, A. Chan, D. Hart, F. Lehner, B. Madden, E. Standen, Study on development of water electrolysis in the EU by E4tech Sàrl with Element Energy Ltd for the Fuel Cells and Hydrogen Joint Undertaking, 2014.

[12] K.E. Ayers, E.B. Anderson, C. Capuano, B. Carter, L. Dalton, G. Hanlon, et al., Research Advances towards Low Cost, High Efficiency PEM Electrolysis, ECS Trans. 33 (2010) 3–15. doi:10.1149/1.3484496.

[13] Fuel Cells and Hydrogen Joint Undertaking, Commercialisation of energy storage in europe, A fact-based analysis of the implications of projected development of the European electric power system towards 2030 and beyond for the role and commercial viability of energy storage, 2015.

[14] L. Bertuccioli, A. Chan, D. Hart, F. Lehner, B. Madden, Eleanor Standen, Development of Water Electrolysis in the European Union, 2014.

[15] K.A. Friedrich, Studie über die Planung einer Demonstrationsanlage zur Wasserstoff - Kraftstoffgewinnung durch Elektrolyse mit Zwischenspeicherung in Salzkavernen, 2015.

[16] H.G. Kim, L.K. Kwa, W. Han, L.K. Kwac, W. Han, The Performance and Stability of a

PEM Electrolyzer Using 3-D Mesh Hong, in: Int. Conf. Power Energy Syst. Lect. Notes Inf. Technol. Vol.13, 2012: pp. 373–379. http://www.ier-institute.org/2070-1918/lnit13/v13/373.pdf.

[17] C.K. Jin, M.G. Jeong, C.G. Kang, Fabrication of titanium bipolar plates by rubber forming and performance of single cell using TiN-coated titanium bipolar plates, Int. J. Hydrogen Energy. (2014) 1–9. doi:10.1016/j.ijhydene.2014.03.013.

[18] A.S. Gago, S.A. Ansar, B. Saruhan, U. Schulz, P. Lettenmeier, N.A. Cañas, et al., Protective coatings on stainless steel bipolar plates for proton exchange membrane (PEM) electrolysers, J. Power Sources. 307 (2016) 815–825. doi:10.1016/j.jpowsour.2015.12.071.

[19] A.S. Gago, A.S. Ansar, P. Gazdzicki, N. Wagner, J. Arnold, K.A. Friedrich, Low Cost Bipolar Plates for Large Scale PEM Electrolyzers, ECS Trans. 64 (2014) 1039–1048. doi:10.1149/06403.1039ecst.

[20] A. Marshall, B. Børresen, G. Hagen, M. Tsypkin, R. Tunold, Hydrogen production by advanced proton exchange membrane (PEM) water electrolysers—Reduced energy consumption by improved electrocatalysis, Energy. 32 (2007) 431–436. doi:http://dx.doi.org/10.1016/j.energy.2006.07.014.

[21] J. Cheng, H. Zhang, G. Chen, Y. Zhang, Study of IrxRu1-xO2 oxides as anodic electrocatalysts for solid polymer electrolyte water electrolysis, Electrochim. Acta. 54 (2009) 6250–6256. doi:10.1016/j.electacta.2009.05.090.

[22] P.C.K. Vesborg, T.F. Jaramillo, Addressing the terawatt challenge: scalability in the supply of chemical elements for renewable energy, RSC Adv. 2 (2012) 7933. doi:10.1039/c2ra20839c.

[23] E.A. Paoli, F. Masini, R. Frydendal, D. Deiana, C. Schlaup, M. Malizia, et al., Oxygen evolution on well-characterized mass-selected Ru and RuO2 nanoparticles, Chem. Sci. 6 (2015) 190–196. doi:10.1039/C4SC02685C.

[24] P. Lettenmeier, L. Wang, U. Golla-Schindler, P. Gazdzicki, N. a Cañas, M. Handl, et al., Nanosized IrOx -Ir Catalyst with Relevant Activity for Anodes of Proton Exchange Membrane Electrolysis Produced by a Cost-Effective Procedure, Angew. Chemie. 55 (2016) 742–746. doi:10.1002/anie.201507626.

[25] H.-S. Oh, H.N. Nong, T. Reier, M. Gliech, P. Strasser, Oxide-supported Ir nanodendrites with high activity and durability for the oxygen evolution reaction in acid PEM water electrolyzers, Chem. Sci. 00 (2015) 1–8. doi:10.1039/C5SC00518C.

[26] H.N. Nong, H.-S. Oh, T. Reier, E. Willinger, W. M.G., V. Petkov, et al., Oxide-Supported IrNiOx Core-Shell Particles as Efficient, Cost-Effective, and Stable Catalysts for Electrochemical Water Splitting, Angew. Chemie. 54 (2015) 2975–2979. doi:10.1002/anie.201411072.

[27] T. Reier, Z. Pawolek, S. Cherevko, M. Bruns, T. Jones, D. Teschner, et al., Molecular Insight in Structure and Activity of Highly Efficient, Low-Ir Ir-Ni Oxide Catalysts for Electrochemical Water Splitting (OER)., J. Am. Chem. Soc. 137 (2015) 13031–40. doi:10.1021/jacs.5b07788.

[28] V.-H. Tran, T. Yatabe, T. Matsumoto, H. Nakai, K. Suzuki, T. Enomoto, et al., An IrSi

oxide film as a highly active water-oxidation catalyst in acidic media, Chem. Commun. 51 (2015) 12589–12592. doi:10.1039/C5CC04286K.

[29] L. Wang, P. Lettenmeier, U. Golla-Schindler, P. Gazdzicki, N.A. Cañas, T. Morawietz, et al., Nanostructured Ir-supported on Ti4O7 as cost effective anode for proton exchange membrane (PEM) electrolyzers, Phys. Chem. Chem. Phys. 18 (2015) 4487–4495. doi:10.1039/C5CP05296C.

[30] H.N. Nong, L. Gan, E. Willinger, D. Teschner, P. Strasser, S. Information, et al., IrOx core-shell nanocatalysts for cost- and energy-efficient electrochemical water splitting, Chem. Sci. 5 (2014) 2955. doi:10.1039/c4sc01065e.

[31] M. Bernicke, E. Ortel, T. Reier, A. Bergmann, J. Ferreira de Araujo, P. Strasser, et al., Iridium Oxide Coatings with Templated Porosity as Highly Active Oxygen Evolution Catalysts: Structure-Activity Relationships., ChemSusChem. 8 (2015) 1908–15. doi:10.1002/cssc.201402988.

[32] R. Frydendal, E.A. Paoli, I. Chorkendorff, J. Rossmeisl, I.E.L. Stephens, Toward an Active and Stable Catalyst for Oxygen Evolution in Acidic Media: Ti-Stabilized MnO 2, Adv. Energy Mater. 5 (2015) n/a–n/a. doi:10.1002/aenm.201500991.

[33] P. Lettenmeier, L. Wang, U. Golla-Schindler, P. Gazdzicki, N. a Cañas, M. Handl, et al., Nanosized IrOx -Ir Catalyst with Relevant Activity for Anodes of Proton Exchange Membrane Electrolysis Produced by a Cost-Effective Procedure, Angew. Chemie. 55 (2015) 742–746. doi:10.1002/anie.201507626.

[34] S.A.A. Grigoriev, V.I.I. Porembskiy, S.V. V Korobtsev, V.N.N. Fateev, F. Auprêtre, P. Millet, High-pressure PEM water electrolysis and corresponding safety issues, Int. J. Hydrogen Energy. 36 (2011) 2721–2728. doi:10.1016/j.ijhydene.2010.03.058.

[35] C. Rozain, P. Millet, Electrochemical characterization of Polymer Electrolyte Membrane Water Electrolysis Cells, Electrochim. Acta. 131 (2014) 160–167. doi:10.1016/j.electacta.2014.01.099.

[36] S. Siracusano, V. Baglio, N. Briguglio, G. Brunaccini, A. Di Blasi, A. Stassi, et al., An electrochemical study of a PEM stack for water electrolysis, Int. J. Hydrogen Energy. 37 (2012) 1939–1946. doi:10.1016/j.ijhydene.2011.06.019.

[37] S. Siracusano, N. Van Dijk, E. Payne-Johnson, V. Baglio, a. S.S. Aricò, Nanosized IrOx and IrRuOx electrocatalysts for the O2 evolution reaction in PEM water electrolysers, Appl. Catal. B Environ. 164 (2015) 488–495. doi:10.1016/j.apcatb.2014.09.005.

[38] P. Millet, D. Dragoe, S. Grigoriev, V. Fateev, C. Etievant, GenHyPEM: A research program on PEM water electrolysis supported by the European Commission, Int. J. Hydrogen Energy. 34 (2009) 4974–4982. doi:10.1016/j.ijhydene.2008.11.114.

[39] H. Ito, T. Maeda, A. Nakano, C.M. Hwang, M. Ishida, A. Kato, et al., Experimental study on porous current collectors of PEM electrolyzers, Int. J. Hydrogen Energy. 37 (2012) 7418–7428. doi:10.1016/j.ijhydene.2012.01.095.

[40] E.A. Paoli, F. Masini, R. Frydendal, D. Deiana, P. Malacrida, T.W. Hansen, et al., Fine-tuning the activity of oxygen evolution catalysts: The effect of oxidation pre-treatment on size-selected Ru nanoparticles, Catal. Today. 262 (2016) 57–64. doi:10.1016/j.cattod.2015.10.005.

[41] N. Danilovic, R. Subbaraman, K.-C. Chang, S.H. Chang, Y.J. Kang, J. Snyder, et al., Activity-Stability Trends for the Oxygen Evolution Reaction on Monometallic Oxides in Acidic Environments., J. Phys. Chem. Lett. 5 (2014) 2474–8. doi:10.1021/jz501061n.

[42] S. Cherevko, T. Reier, A.R. Zeradjanin, Z. Pawolek, P. Strasser, K.J.J. Mayrhofer, Stability of nanostructured iridium oxide electrocatalysts during oxygen evolution reaction in acidic environment, Electrochem. Commun. 48 (2014) 81–85. doi:10.1016/j.elecom.2014.08.027.

[43] P. Millet, A. Ranjbari, F. de Guglielmo, S.A. Grigoriev, F. Auprêtre, Cell failure mechanisms in PEM water electrolyzers, Int. J. Hydrogen Energy. 37 (2012) 17478–17487. doi:10.1016/j.ijhydene.2012.06.017.

[44] S. Sun, Z. Shao, H. Yu, G. Li, B. Yi, Investigations on degradation of the long-term proton exchange membrane water electrolysis stack, J. Power Sources. 267 (2014) 515–520. doi:10.1016/j.jpowsour.2014.05.117.

[45] M. a. Travassos, V. V. Lopes, R. a. Silva, a. Q. Novais, C.M. Rangel, Assessing cell polarity reversal degradation phenomena in PEM fuel cells by electrochemical impedance spectroscopy, Int. J. Hydrogen Energy. 38 (2013) 7684–7696. doi:10.1016/j.ijhydene.2013.01.132.

[46] D. Malevich, E. Halliop, B. a. Peppley, J.G. Pharoah, K. Karan, Investigation of Charge-Transfer and Mass-Transport Resistances in PEMFCs with Microporous Layer Using Electrochemical Impedance Spectroscopy, J. Electrochem. Soc. 156 (2009) B216. doi:10.1149/1.3033408.

[47] J.T. Mueller, P.M. Urban, Characterization of direct methanol fuel cells by ac impedance spectroscopy, J. Power Sources. 75 (1998) 139–143. doi:10.1016/S0378-7753(98)00109-8.

[48] O. Antoine, Y. Bultel, R. Durand, Oxygen reduction reaction kinetics and mechanism on platinum nanoparticles inside Nafion®, J. Electroanal. Chem. 499 (2001) 85–94. doi:10.1016/S0022-0728(00)00492-7.

[49] M. Eikerling, a. a. Kornyshev, Electrochemical impedance of the cathode catalyst layer in polymer electrolyte fuel cells, J. Electroanal. Chem. 475 (1999) 107–123. doi:10.1016/S0022-0728(99)00335-6.

[50] S.A. Grigoriev, K.A. Dzhus, D.G. Bessarabov, P. Millet, Failure of PEM water electrolysis cells: Case study involving anode dissolution and membrane thinning, Int. J. Hydrogen Energy. 39 (2014) 20440–20446. doi:http://dx.doi.org/10.1016/j.ijhydene.2014.05.043.

[51] S. Stucki, G.G. Scherer, S. Schlagowski, E. Fischer, PEM water electrolysers: evidence for membrane failure in 100 kW demonstration plants, J. Appl. Electrochem. 28 (1998) 1041–1049.

[52] W.K. Liu, S.J.C. Cleghorn, B.E. Delaney, M. Crum, Chemical and mechanical membrane degradation, in: Handb. Fuel Cells, John Wiley & Sons, Ltd, 2010. doi:10.1002/9780470974001.f500028.

[53] A. Laconti, H. Liu, C. Mittelsteadt, R. McDonald, Polymer Electrolyte Membrane Degradation Mechanisms in Fuel Cells - Findings Over the Past 30 Years and Comparison

with Electrolyzers, in: ECS Trans., ECS, 2006: pp. 199–219. doi:10.1149/1.2214554.

[54] V. a. Sethuraman, J.W. Weidner, A.T. Haug, S. Motupally, L. V. Protsailo, Hydrogen Peroxide Formation Rates in a PEMFC Anode and Cathode, J. Electrochem. Soc. 155 (2008) B50. doi:10.1149/1.2801980.

[55] E. Guilminot, A. Corcella, M. Chatenet, F. Maillard, F. Charlot, G. Berthomé, et al., Membrane and Active Layer Degradation upon PEMFC Steady-State Operation, J. Electrochem. Soc. 154 (2007) B1106. doi:10.1149/1.2775218.

[56] S. Helmly, B. Ohnmacht, P. Gazdzicki, R. Hiesgen, E. Gülzow, K.A. Friedrich, Influence of the Distribution of Platinum Deposits on the Properties and Degradation of Platinum-Impregnated Nafion Membranes, J. Electrochem. Soc. 161 (2014) F1416–F1426. doi:10.1149/05801.0969ecst.

[57] P.J. Ferreira, G.J. la O', Y. Shao-Horn, D. Morgan, R. Makharia, S. Kocha, et al., Instability of Pt/C Electrocatalysts in Proton Exchange Membrane Fuel Cells, J. Electrochem. Soc. 152 (2005) A2256. doi:10.1149/1.2050347.

[58] J. Aragane, Change of Pt Distribution in the Active Components of Phosphoric Acid Fuel Cell, J. Electrochem. Soc. 135 (1988) 844. doi:10.1149/1.2095790.

[59] J. Aragane, H. Urushibata, T. Murahashi, Effect of operational potential on performance decay rate in a phosphoric acid fuel cell, J. Appl. Electrochem. 26 (1996) 147–152. doi:10.1007/BF00364064.

[60] J. Xie, D.L. Wood, K.L. More, P. Atanassov, R.L. Borup, Microstructural Changes of Membrane Electrode Assemblies during PEFC Durability Testing at High Humidity Conditions, J. Electrochem. Soc. 152 (2005) A1011. doi:10.1149/1.1873492.

[61] R.A. Silva, T. Hashimoto, G.E. Thompson, C.M. Rangel, Characterization of MEA degradation for an open air cathode PEM fuel cell, Int. J. Hydrogen Energy. 37 (2012) 7299–7308. doi:10.1016/j.ijhydene.2011.12.110.

[62] F.A. de Bruijn, V.A.T. Dam, G.J.M. Janssen, Review: Durability and Degradation Issues of PEM Fuel Cell Components, Fuel Cells. 8 (2008) 3–22. doi:10.1002/fuce.200700053.

Figure Captions

Figure 1: Protocol of measurements of the 8-cell 120 cm² stack: a) Input current density; b) Output stack potential. EIS was measured at the time steps T1, T2 and T3 of the protocol.

Figure 2: a) Polarization curve of all cells up to 4 A cm^{-2} and the corresponding stack temperature; b) Initial EIS for each cell from 1 kHz to 100 mHz at 30 A and 29 °C and c) Activation resistances of each cell.

Figure 3: a) Cell potential (E_{cell}) of Cell 7 and 8 at 2 A cm^{-2} for 400 h; cb E_{cell} of Cell 7 and 8 at 4 A cm^{-2} for 250 h; c) E_{cell} of all cells measured at 2 A cm^{-2} after T1, T2 and T3 (refer to protocol of Figure 1).

Figure 4: a) Equivalent circuit for simulating the EIS; b) Impedance spectra for cell 7 at 29 °C, at a current density 0.25A cm^{-2} (30 A) measured at T1, T2, and T3 (Figure 1). The continuous line shows the fit of equivalent circuit above. c) Measurement and the simulation fit of cell 7 at 2, 5, 10, 20, 30, 40 A and 30°C. The EIS frequencies ranged from 1 kHz to 100 mHz.

Figure 5: a) Polarization curves of cell 7 up to 2 A cm^{-2} at T1, T2 and T3 recorded with HHG rectifier and temperature corrected with 5.5 mV $°C^{-1}$; b) Low current density part of the polarization curve of cell 7 recorded with a potentiostat during EIS measurements; c) Activation overpotential and d) the resulting ohmic overpotential measured at 2, 5, 10, 20, 30 and 40 A.

Figure 6: Cross-section SEM images of a) and c) the E500 MEA before tests; b), e) Cell 8 and d) Cell 7 after tests or post-mortem.

Figure 7: Conductive AFM measurements: a) Initial anode (cell 7); b) Cell 7 anode; c) Cell 8 anode; d) Initial cathode; e) Cell 7 cathode; f) Cell 8 cathode. Current range: 0-250 pA.

Fig. 1

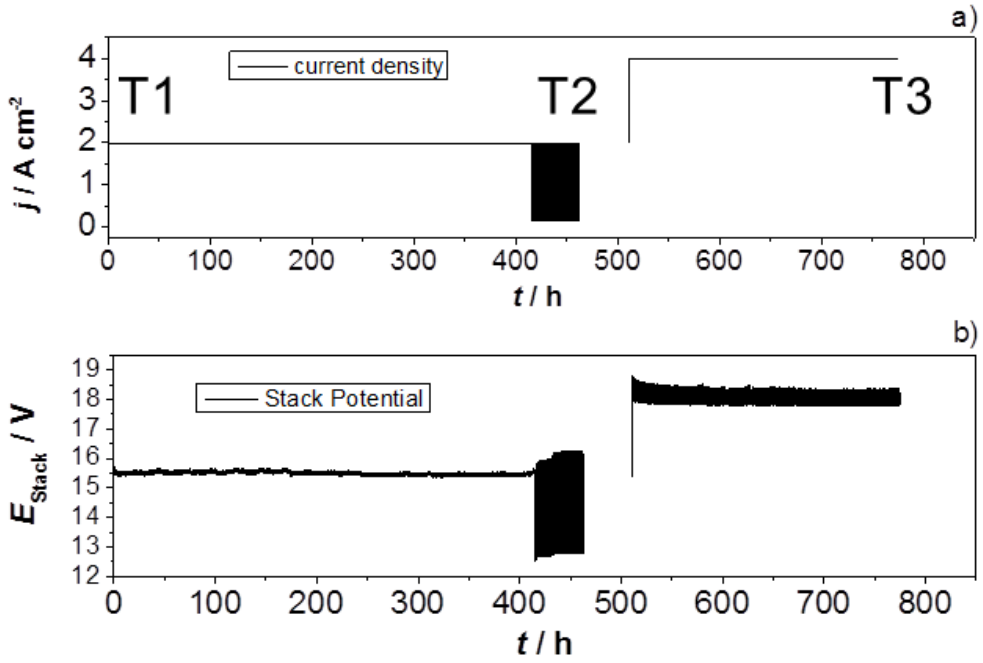

Fig. 2

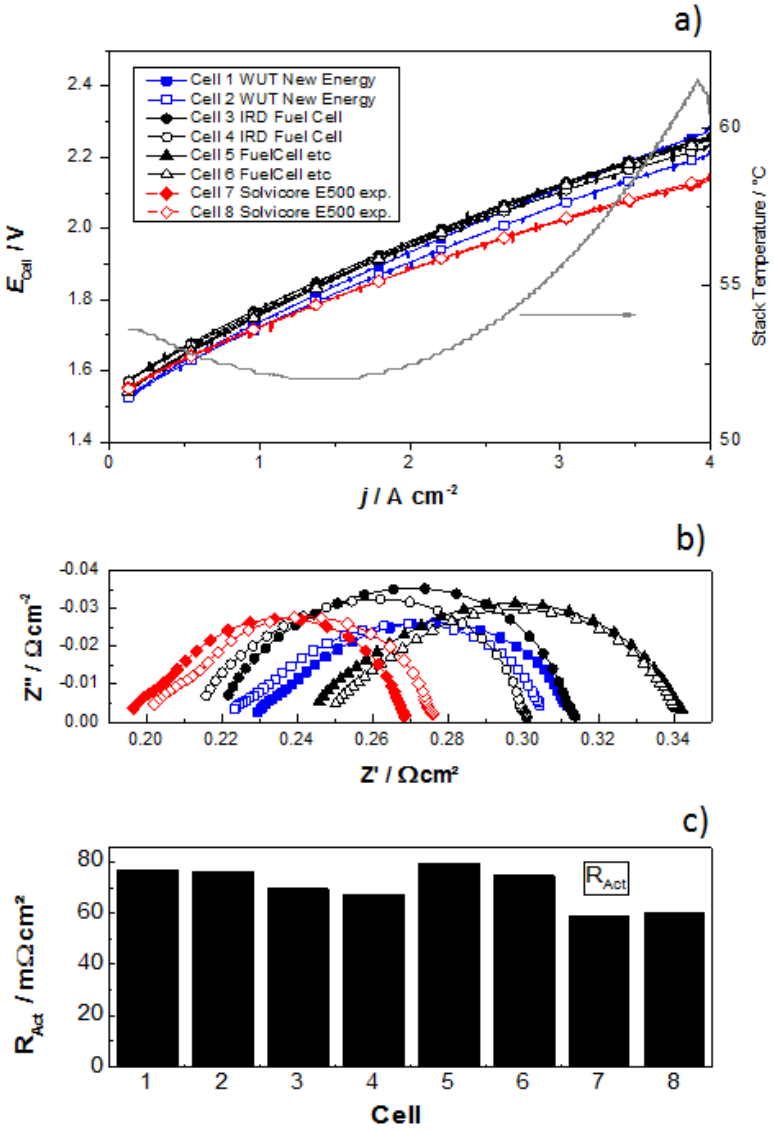

Fig. 3

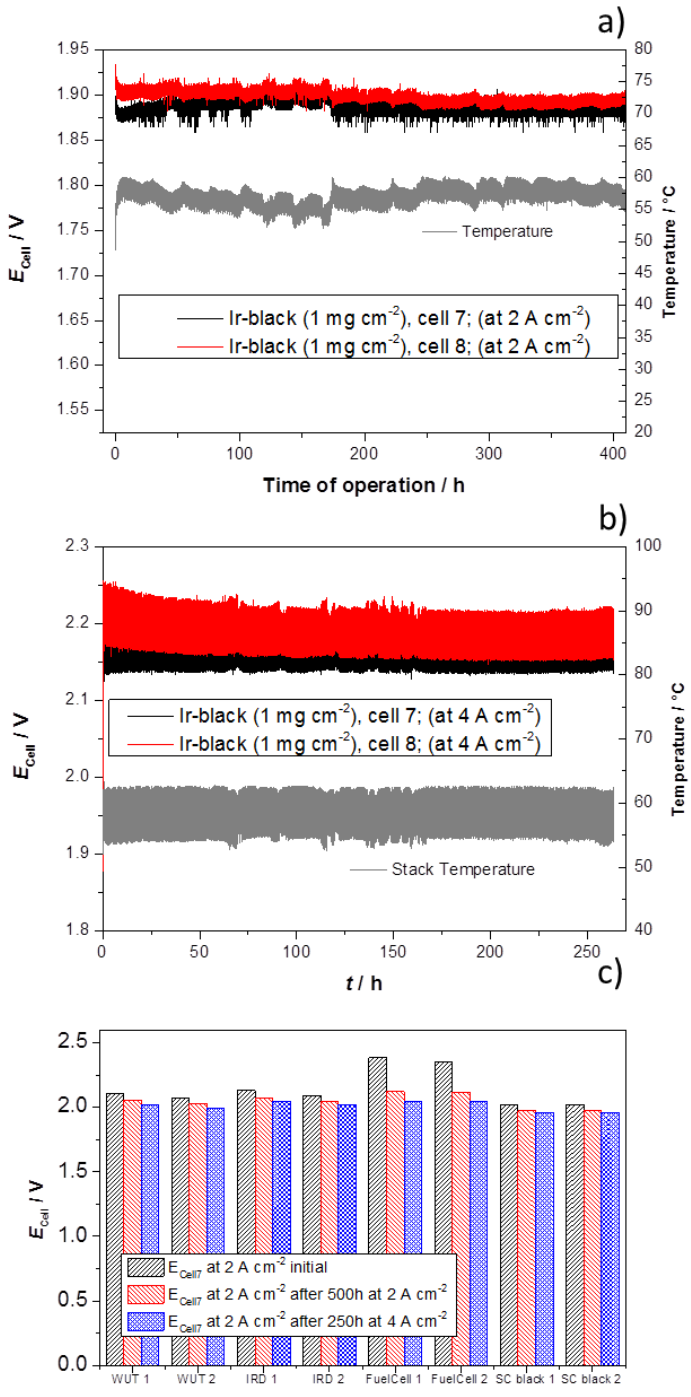

Fig. 4

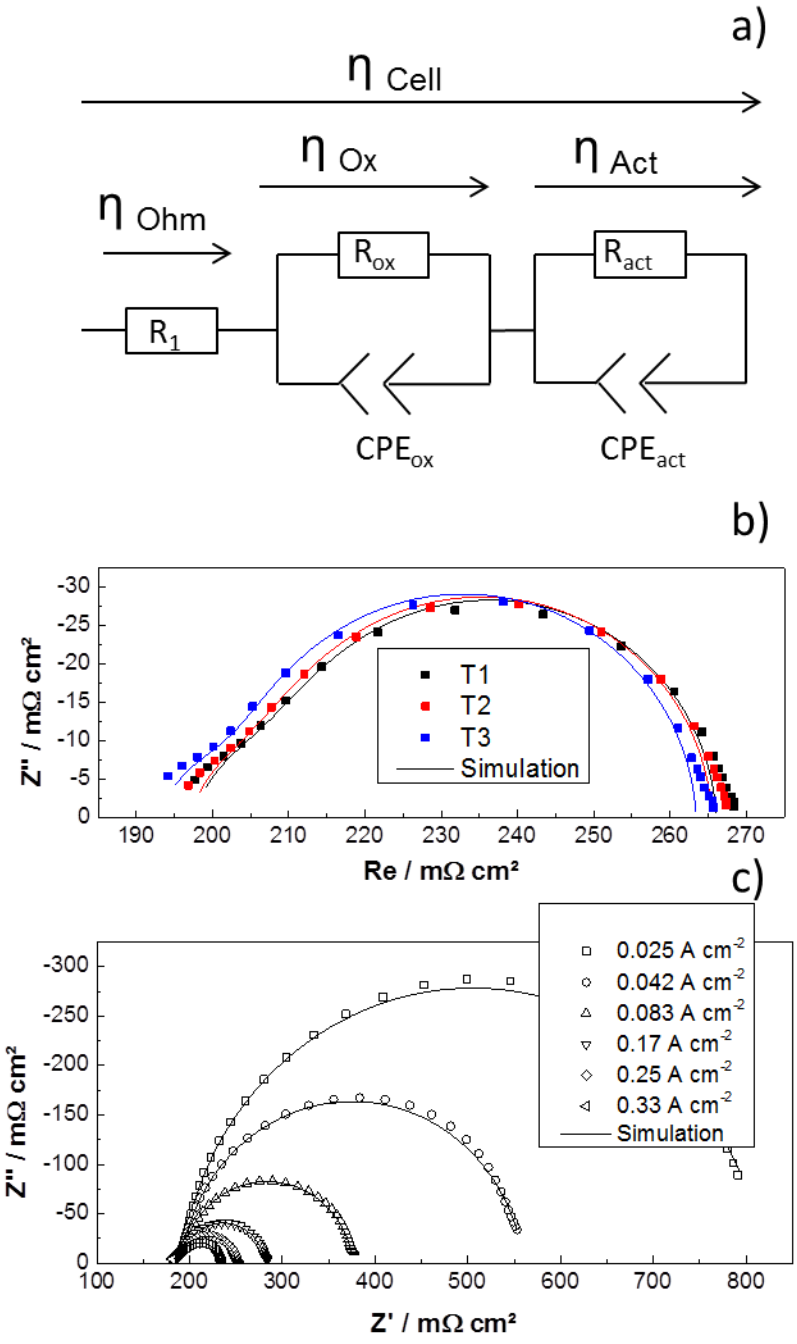

Fig. 5

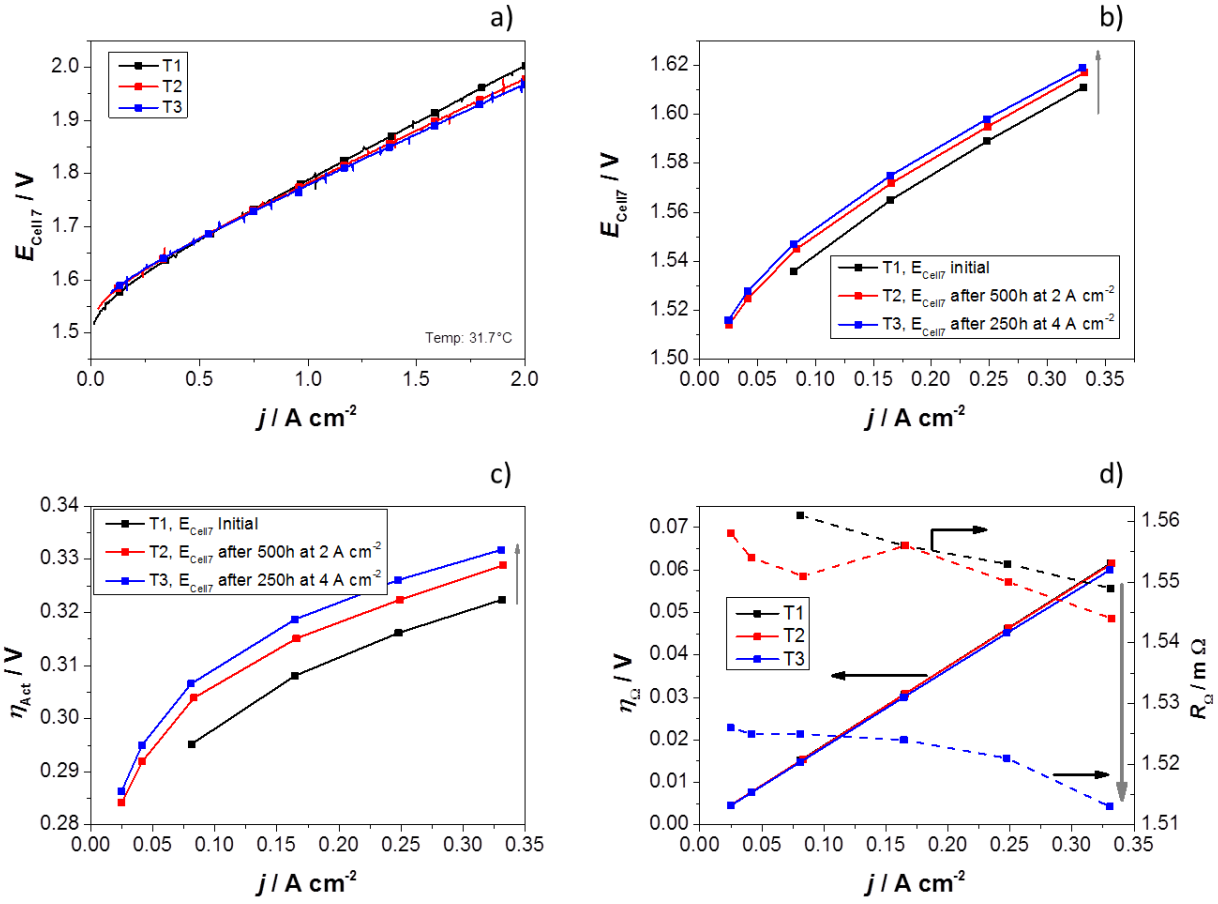

Fig. 6

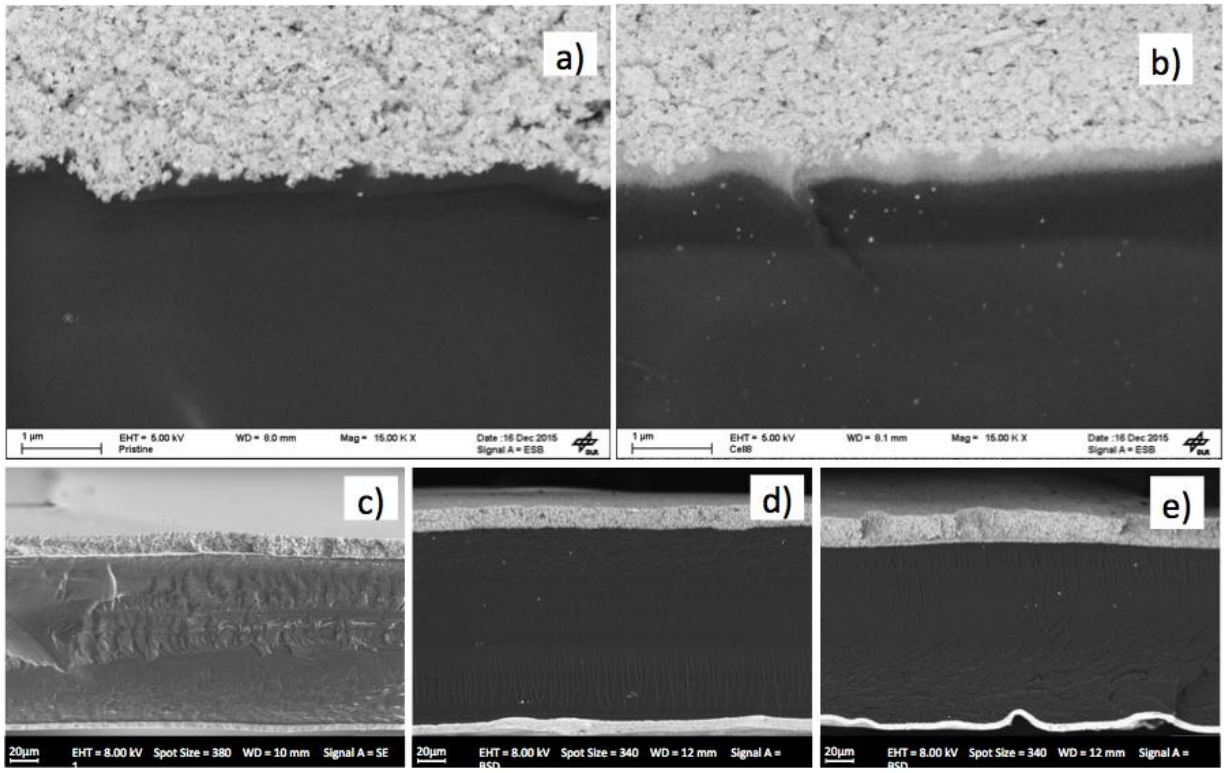

Fig. 7

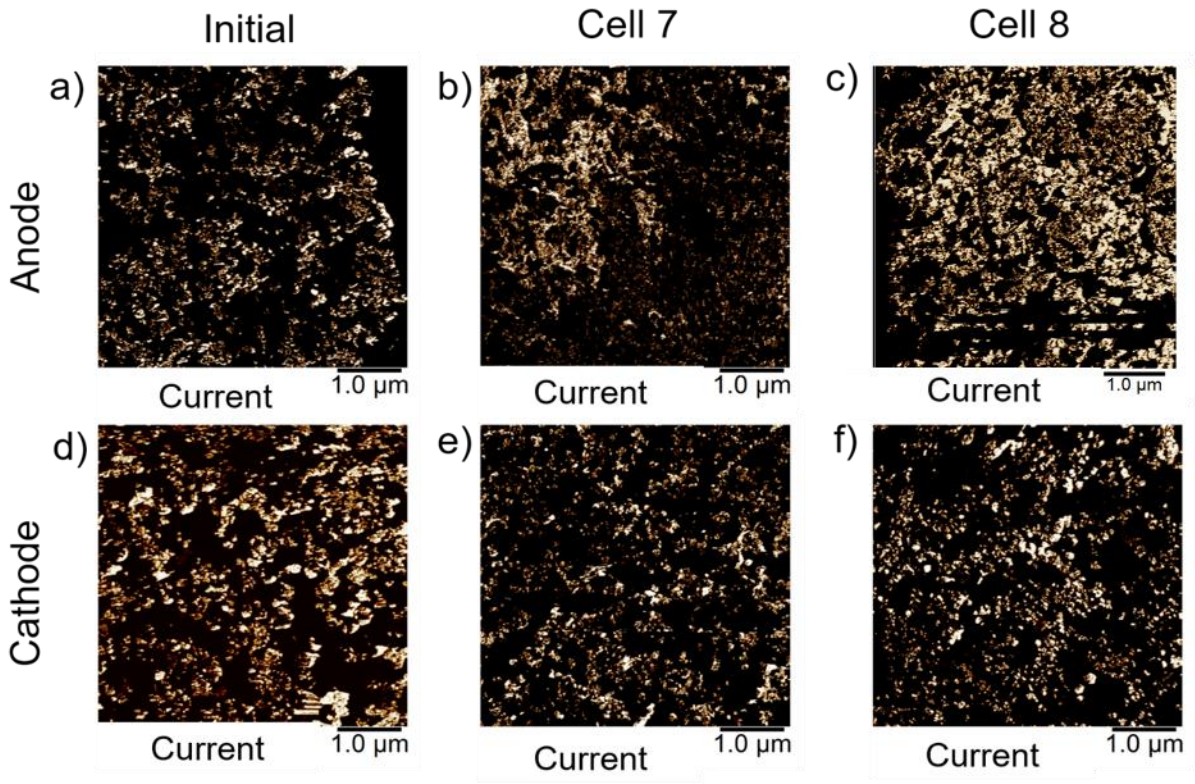

Tables

Table 1. Arrangement of MEAs in the 120 cm^2 PEM electrolyzer stack.

Cell	MEA Provider	Anode catalyst; loading (mg cm^{-2})	Membrane	Cathode catalyst; loading (mg cm^{-2})
1 and 2	Wuhan WUT New	IrO_2; 2	N 115	Pt; 0.8
3 and 4	IRD	IrO_2:coarse Ir; 0.3:2	N 115	60w% Pt/C; 0.5
5 and 6	FuelCellsEtc	Ir; 3	N 115	Pt; 3
7 and 8	Solvicore E500	Ir-black (Umicore); 1	N 115	Pt; 0.9

Table 2. Tafel slope (β) and specific exchange current (i_0) of Ir-black recorded by rotating disc electrode (RDE) measurements in Ar-saturated 0.5 M H_2SO_4, at a scan rate of 5mV s^{-1} and a rotating speed of 2300 rpm. For comparison, the parameters of the E500 (Cell 7) calculated from the kinetic arc of EIS at different current densities are included

Anode catalyst / MEA	**T / °C**	**β /mV**	**i_0 / 10^{-9} A mg_{Ir}^{-1}**
RDE in Ar-saturated 0.5 M H2SO4	30	43,1	3
T1 – E500 initial	30	44.3	18.1
		41.3[a]	5.5[a]
T2 - E500 after 2 A cm^{-2} (500 h)	30	41.1	3.5
T3 - E500 after 4 A cm^{-2} (250 h)	30	41.1	2.8

[a] after correction to achieve comparable tafel slope.

Table 3. XPS measurements of DI water resin of the anodic water cycle. It is presented the fresh resin and the average values of two measurements of the used resin, from the bottom and from the top of the resin container.

Element	**Fresh [wt%]**	**Used [wt%]**
Fe	0.0	2.6
F	0.0	2.9
O	10.9	21.4
Ti	0.0	2.7
N	2.4	3
C	79.6	52.9
S	7.2	9.9
Si	0.0	3.3
Ir	0.0	1.3

Table 4: Conductive area of the electrodes of the MEAs and average thickness of the layers before and after tests.

	Conductive area (%)			Average Thickness / µm		
	unused	Cell 7 (used)	Cell 8 (used)	unused	Cell 7 (used)	Cell 8 (used)
Anode	30 ± 4	47 ± 2	45 ± 5	5 ± 0.4	4.98 ± 0.3	4.3 ± 0.6
Cathode	37 ± 2	38 ± 3	39 ± 5	16.1 ± 0.6	14.8 ± 2.3	16.7 ± 1
Membrane				121.5 ± 1.5	129.8 ± 1.6	137.4 ± 2.9